Flexible organic crystals. Understanding the tractable co-existence of elastic and plastic bending

Indira S. Divya, Saravanan Kandasamy, Shodai Hasebe, Toshiyuki Sasaki,

Hideko Koshima,* Krzysztof Woźniak* and Sunil Varughese*

Supporting Information

Experimental details

Synthesis of oxalates:

Diphenyl oxalate derivatives were prepared from para halo substituted phenols (15 mmol) and oxalyl chloride (7.5 mmol) using trimethylamine (15 mmol) in dry DCM (20 ml) and stirred for 3 hours in ice bath. White solid formed extracted with DCM and dried. Further Purified by crystallization. The Benzil compounds were obtained from Aldrich Chemicals and were used without further purification. The solvents employed were of spectroscopic grade and slow evaporation methods yielded the crystals suitable for mechanical bending.

Optical and Hot-Stage Microscope (HSM). Melting point determination were performed on a Leica DM 2500 P optical transmission microscope. The apparatus was equipped with a wide zoom camera and Mettler Toledo hot-stage. The crystalline samples were placed on a micro slide, inserted in the hot stage, and observed under the microscope. Images were recorded on heating in the same temperature regions where phase transitions were observed in DSC. The heating rate was 5ºC/min.

Three-point bending experiments

Three-point bending test experiments were conducted by using a universal material testing machine (Tensilon RTG-1210, A&D Co. Ltd.) at ambient conditions (20 °C). The single crystal was mounted on two-point support (copper wires) on copper blocks, and then force (load) was applied to the center of the specimens with a metal jig with a moving speed of 1 mm min^{-1}.

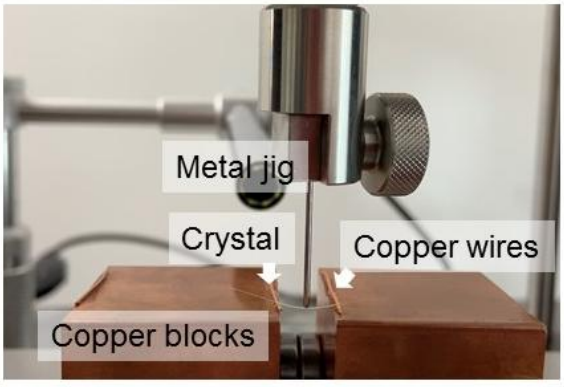

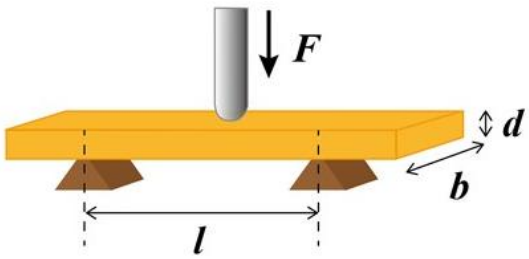

D: maximum deflection of the center of the beam

$$Stress = \frac{3Fl}{2bd^2} \quad Strain = \frac{6Dd}{l^2}$$

$$Young's\ modulus = \frac{Stress}{Strain}$$

Differential Scanning Calorimetry (DSC): The crystallization and melting behavior of samples were analyzed using a differential scanning calorimeter (TA Q2000). About 3 mg of each sample was accurately weighed in aluminum pans and subjected to the thermal scan from room temperature to 150^{o}C at a rate of 5^{o}C/min.

Single crystal X-ray Diffraction: The diffraction data of single crystals were collected on a Bruker Apex-II diffractometer using graphite monochromated Mo-Kα radiation. The data was processed with the SMART software suite. The structure solution was carried out by direct methods, and the refinements were performed by full-matrix least-squares on *F*2 using the SHELXTL suite of programs.

Hirshfeld surface analysis: Hirshfeld surface 2D fingerprint plot was constructed using Crystal Explorer (Ver. 17.5, University of Western Australia). The intermolecular interaction and energy frameworks were calculated at B3LYP/6-31G(d,p) level of dispersion-corrected density functional theory basis set. The energy framework was constructed based on the total intermolecular interaction energy, inclusive of electrostatic, polarization, dispersion and exchange-repulsion components.

Molecular Electrostatic Potential (MESP) Analysis: Theoretical calculations were carried out in Gaussian 16. We optimized the molecules and calculated their MESPs with a DFT method at the level of B3LYP/6-311+G(d,p) till the Br-derivatives and B3LYP/DGDZVP for the I-derivatives. MESP for individual molecules was visualized in GaussView 6.0. NCI analysis was carried out in the Multiwfn 3.7 software, visualized in VMD, and plotted using GNU plot.

Absorption & Emission spectra

The UV-Vis range of 200 to 700 nm wavelength was measured using a spectrophotometer (SHIMADZU UV-2401PC, Shimadzu Japan) by sandwiching the crystalline sample between two quartz plates. The fluorescence spectra were recorded on a SPEX-Fluorolog-3 FL3−221 spectrofluorimeter (excitation wavelengths for BZF, BZC & BZB - 411nm, BZF_O - 375 nm, respectively). In the solid-state, the sample was ground with $BaSO_4$, and the absolute quantum yield was calculated by the integrating sphere (Quanta-φ, Horiba) method.

Table S1 Melting Points of the crystalline compounds

Compound	Melting point(°C)
BZ	94-98
BZF_O	118-122
BZF	117-120
BZC	196-197
BZB	228-229
BZI	243-245
OXH	138-140
OXF	150-154
OXC	183-187
OXB	188-190
OXI	199-205

Table S2 Unit cell parameters of the new polymorph **BZF**

Compound	BZF
Formula	C_{14} H_8 F_2 O_2
CCDC Nos.	2142844
Formula Wt.	246.20
Crystal habit	Acicular
Crystal colour	Pale yellow
Crystal system	Orthorhombic
Space group	$P2_12_12$
a (Å)	6.142(3)
b(Å)	23.249(14)
c (Å)	4.015(2)
α (º)	90
β (º)	90
γ (º)	90
V (Å^3)	573.33(5)
Z	2
*D*calc(g cm^{-3})	1.426
T(K)	298(2)
(λ)Mo Kα	0.71073
μ(mm^{-1})	0.117
2θ range (º)	54.98
Total Reflns.	7181
Unique Reflns.	1315
Reflns. Used	987
No. Parameters	82
GOF on F^2	1.119
Final *R*1, *wR*2	0.0411,0.0943

Table S3 Unit cell parameters of the crystals studied for comparative analysis

Compounds	**BZH**	**BZF_O**	**BZC**	**BZB**	**BZI**
Formula	$C_{14}H_{10}O_2$	$C_{14}H_8F_2O_2$	$C_{14}H_8Cl_2O_2$	$C_{14}H_8Br_2O_2$	$C_{14}H_8I_2O_2$
Space group	*P* 3_121	*P* 2_1/c	*P* 2/n	$P2_12_12$	$P2_12_12$
***a* (Å)**	8.360(2)	12.135(2)	6.029(2)	6.006(12)	5.878(8)
***b* (Å)**	8.360(2)	7.350(1)	3.869(1)	26.006(5)	27.12(4)
***c* (Å)**	13.406(3)	13.157(2)	25.320(8)	4.0378(8)	4.147(4)
***α* (°)**	90	90	90	90	90
β (°)	90	110.51(1)	92.00(2)	90	90
***γ* (°)**	120	90	90	90	90
Z	3	4	2	2	2
CSD Ref Code.	BENZIL07	YODPOX	UVEKOW	EFUZIP01	UVEKUC

Table S3 (contd…)

Compounds	**OXH**	**OXF**	**OXC**	**OXB**	**OXI**
Formula	$C_{14}H_{10}O_4$	$C_{14}H_8F_2O_4$	$C_{14}H_8Cl_2O_4$	$C_{14}H_8Br_2O_4$	$C_{14}H_8I_2O_4$
Space group	*P* $2_1/n$	*P* $2_1/c$	*P* $2_1/c$	*P* $2_1/c$	*C c*
***a* (Å)**	10.622(2)	6.898(14)	12.480(3)	12.054(2)	9.555(19)
***b* (Å)**	7.836(1)	11.480(2)	3.810(8)	3.976(8)	9.679(19)
***c* (Å)**	14.084(2)	8.376(17)	14.151(3)	14.204(3)	31.313(6)
***α* (°)**	90	90	90	90	90
***β* (°)**	103.62(1)	110.79(3)	96.90(3)	94.53(3)	97.02(3)
***γ* (°)**	90	90	90	90	90
Z	4	2	2	2	8
CCDC Ref Code.	HEKTUM	SEJSIM	LAQKIA	SEJSOS	SEJSUY

Table S4 Bending strain calculation

Compound	**Elastic strain**	**Elastic recovery I**†	**Elastic recovery II**‡
BZB	2.45	2.6	1.26
BZC	2.39	3.5	2.58
BZF	2.36	3.35	3.19
OXC	1.05	1.1	2.39
OXB	1.18	0.71	0.82

† Corresponds to the partial recovery of the crystals beyond the elastic limit

‡ Corresponds to the residual recovery even when the crystals are plastically deformed

Calculation of elastic strain using the Euler-Bernoulli's beam bending theory

BZB

Stage-1 ***Stage-2*** ***Stage-3***

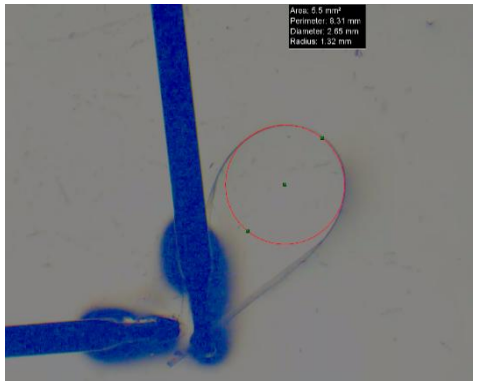

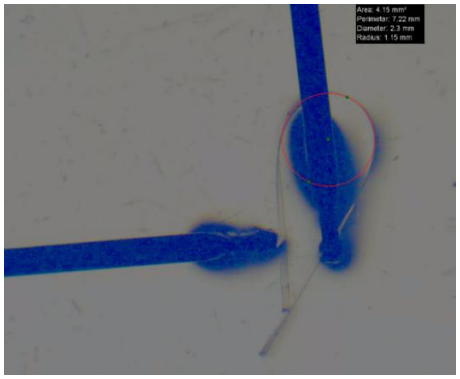

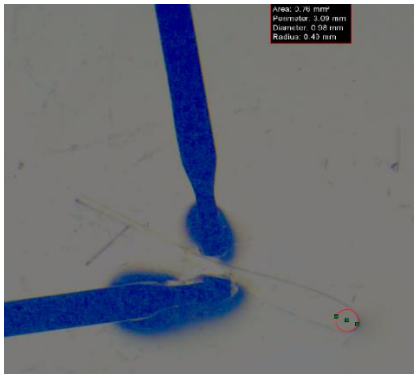

ε = 0.065/ 2.65 = 2.45 %

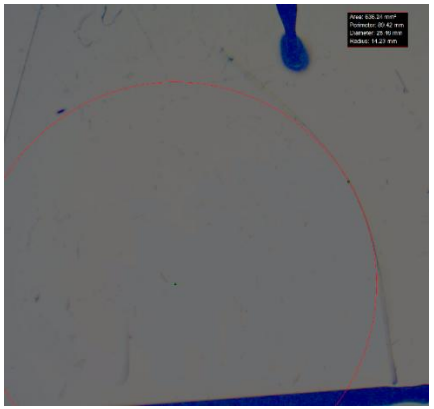

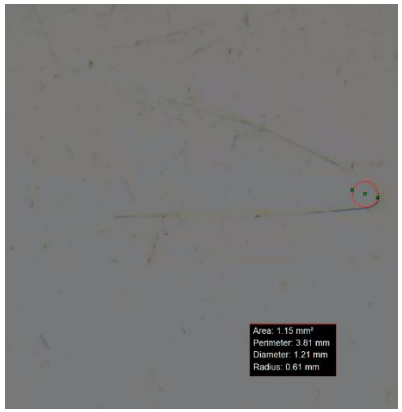

Elastic recovery = ~ 2.6% **Elastic recovery = ~ 1.26%**

Fig. S1 Calculation of elastic strain, percentage of elastic recovery after plastic deformation at the different stages of the mechanical bending of BZB.

BZC

Stage-1

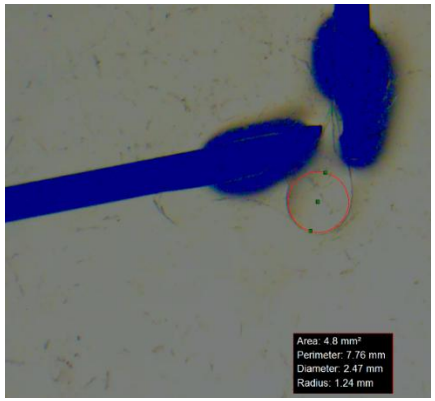

ε = 0.059/ 2.47 = 2.39 %

Stage-2

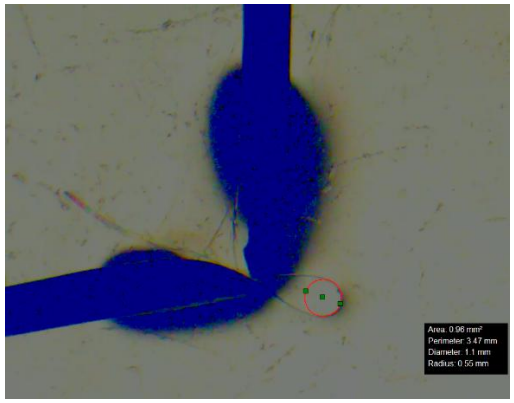

Elastic recovery = ~ 3.5%

Stage-3

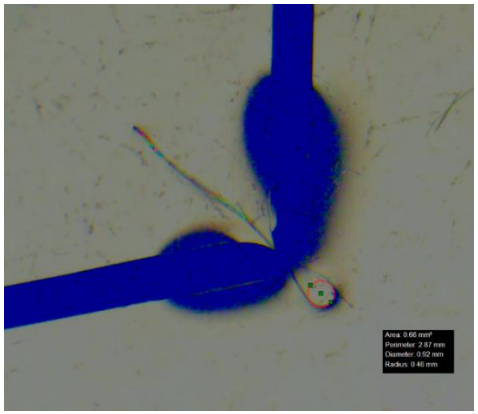

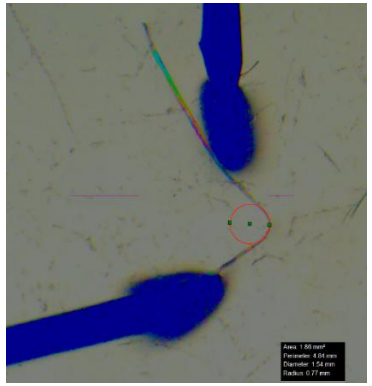

Elastic recovery = ~ 1.26%

Fig. S2 Calculation of elastic strain, percentage of elastic recovery after plastic deformation at the different stages of the mechanical bending of BZC..

BZF

Stage-1 ***Stage-2*** ***Stage-3***

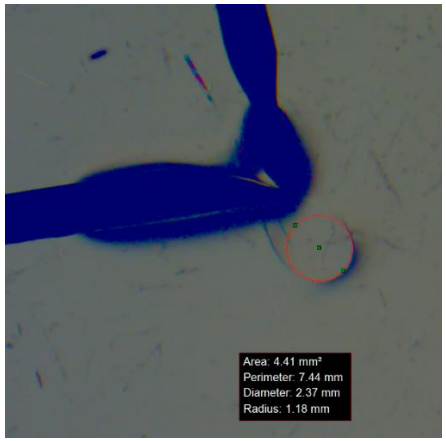

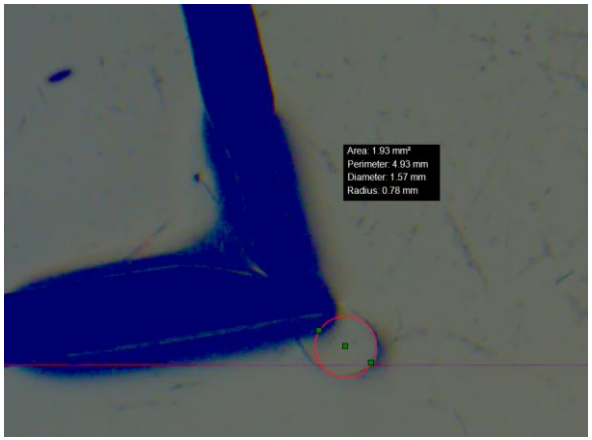

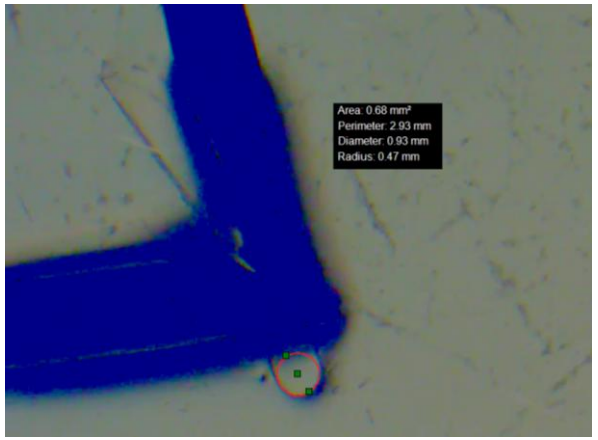

ε = 0.056/ 2.37 = 2.36%

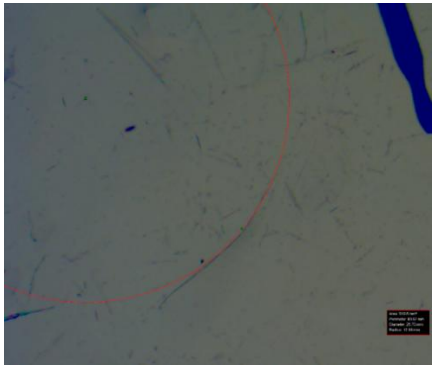

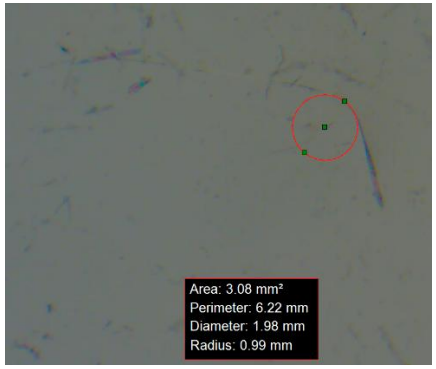

Elastic recovery = ~ 3.35% **Elastic recovery = ~ 3.19%**

Fig. S3 Calculation of elastic strain, percentage of elastic recovery after plastic deformation at the different stages of the mechanical bending of BZF.

Hot-stage microscopy (HSM) images

(a)

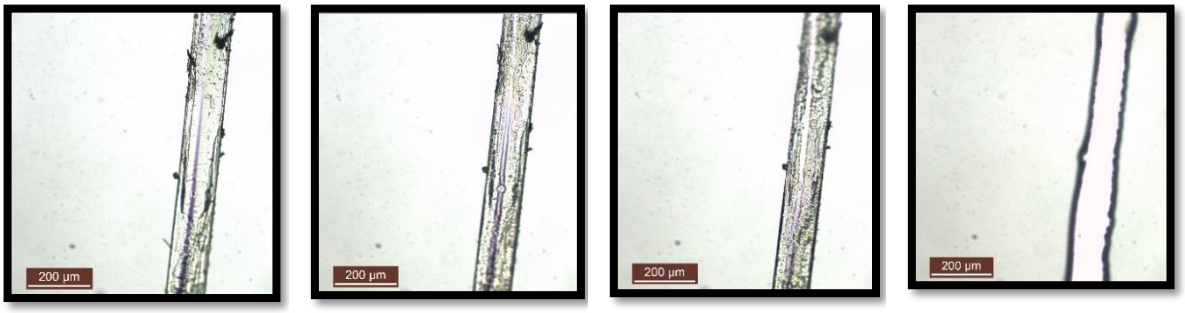

40 **100** **117** **120**

The crystal melting recorded in °C. It melts in the temperature range of 117-120 °C

(b)

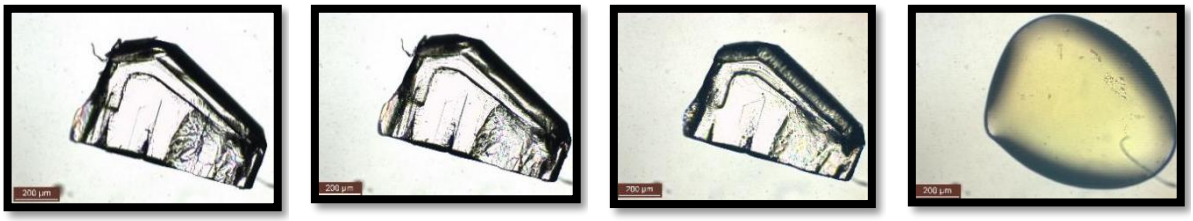

40 **100** **118** **122**

The crystal melting recorded in °C. It melts in the temperature range of 118-122 °C

Fig. S4 Hot-stage microscopy images showing the thermal characteristics of the dimorphs (a) BZF and (b) BZF_O

DSC thermogram

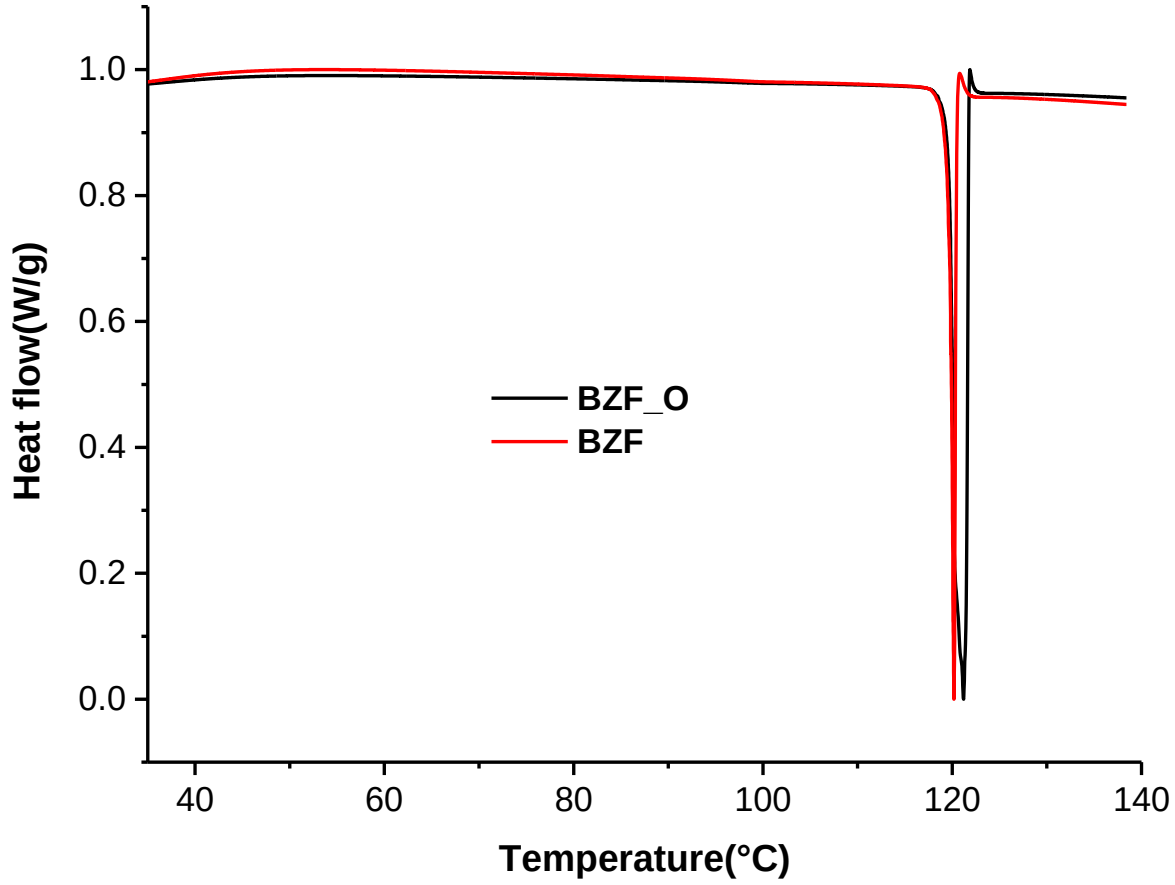

Fig. S5 DSC thermogram of BZF_O and BZF

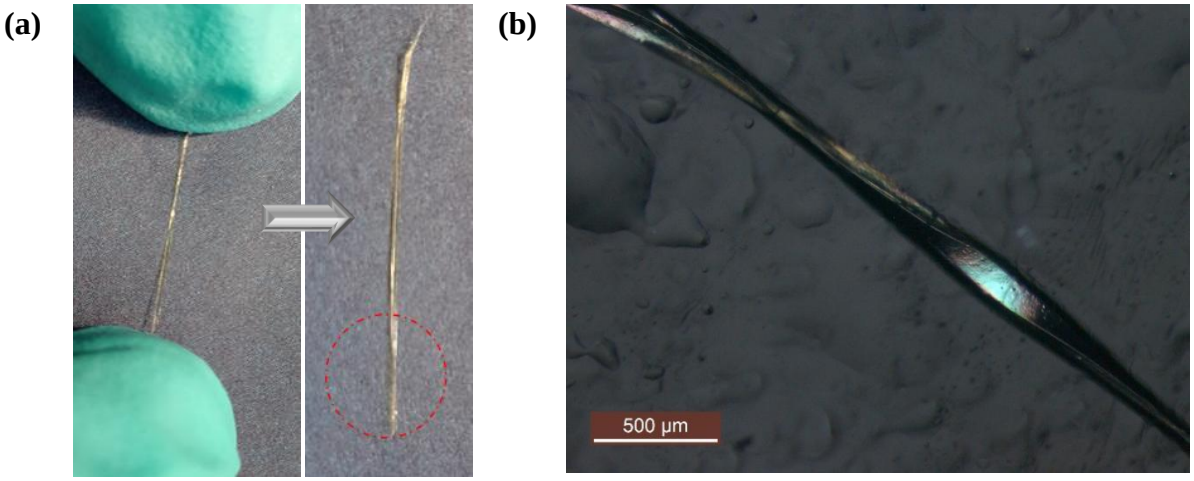

Fig. S6 Twisted crystals of **BZF** (a) Hand twisted crystal (b) out of plane wrapping

BZF **BZF_O**

(a) **(b)**

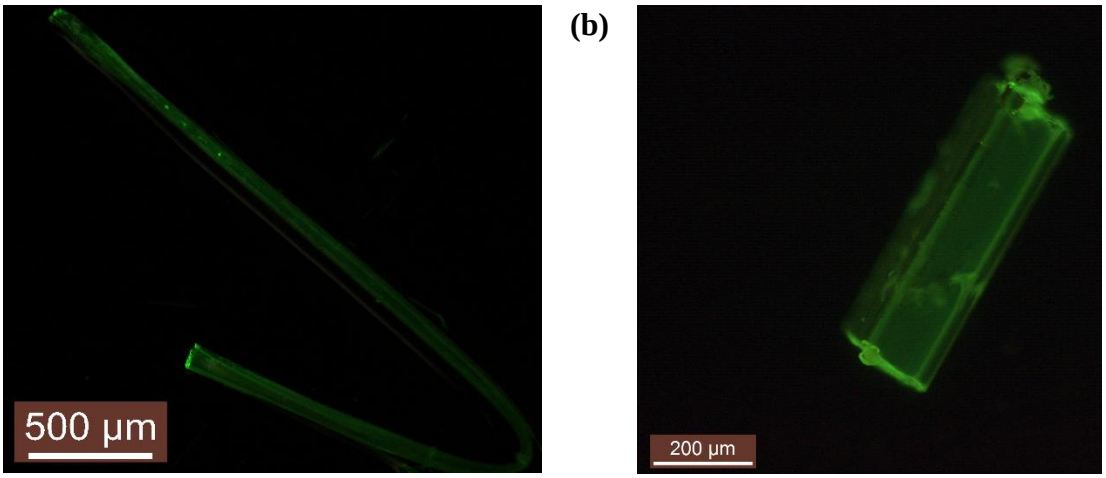

Fig. S7 Fluorescent images of the dimorphs of the F-derivative of benzil: (a)BZF (b)BZF_O. Note the lightened ends of the crystals.

(a)

(b)

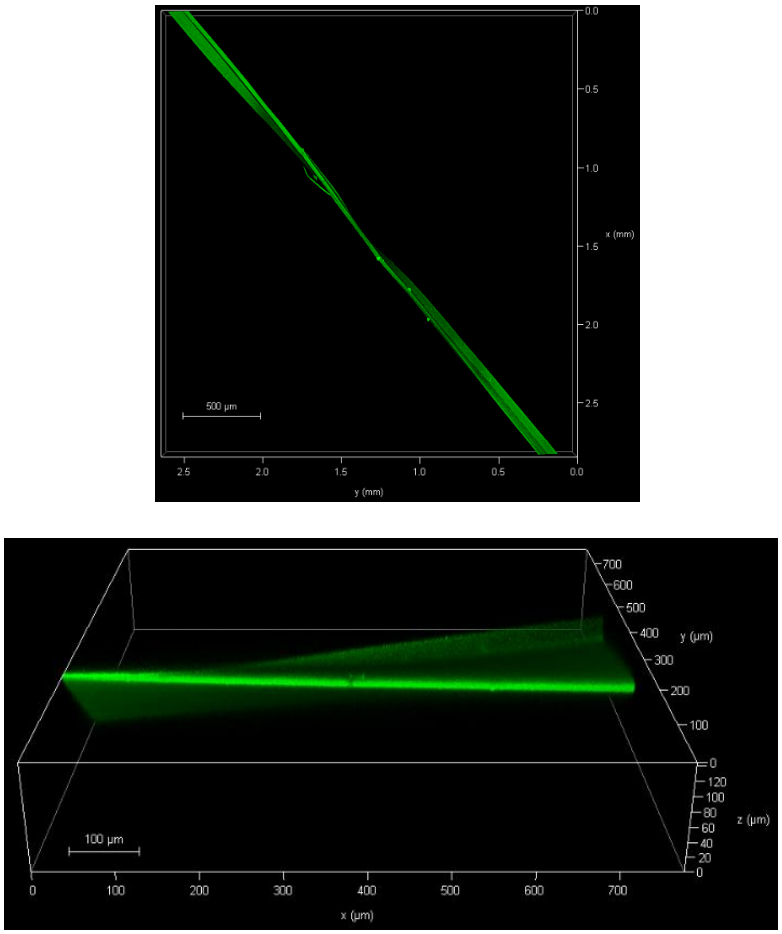

Fig. S8 Additional confocal microscopy images highlighting the twisted nature of the crystals of (a) BZC and (b) BZF (note the out of plane bending in the twisted crystal).

Calculation of elastic strain using the Euler-Bernoulli's beam bending theory

OXB

Stage-1

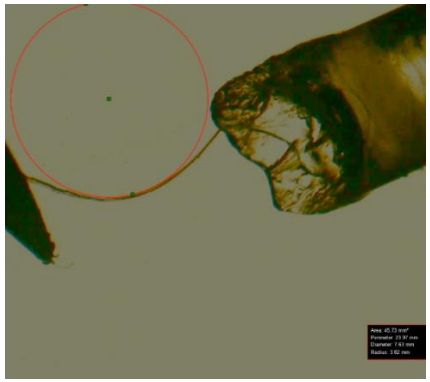

ε **= 0.09/ 7.63 = 1.18 %**

Stage-2

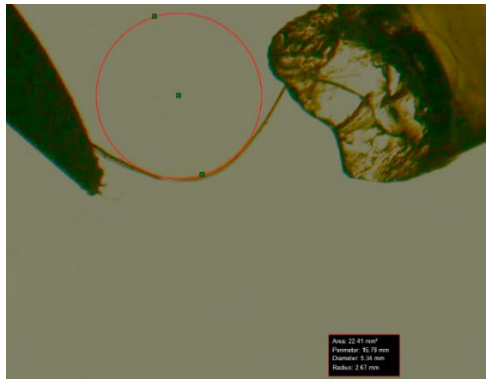

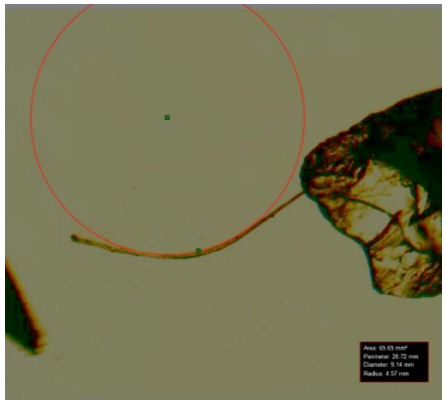

Elastic recovery = ~ 0.71%

Stage-3

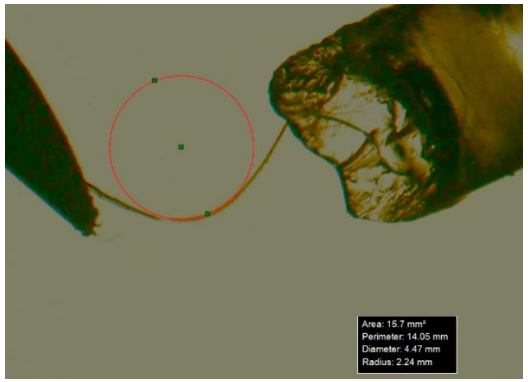

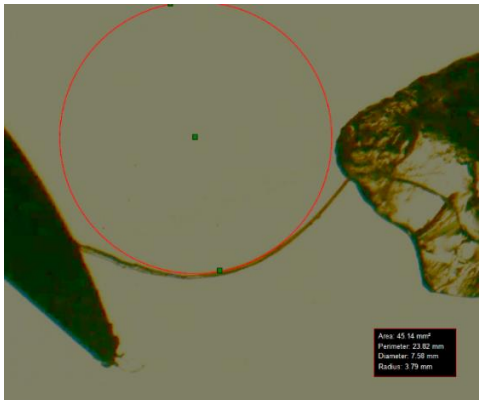

Elastic recovery = ~ 0.83%

Fig. S9 Calculation of elastic strain, percentage of elastic recovery after plastic deformation at the different stagesof the mechanical bending of OXB.

OXC

Stage-1

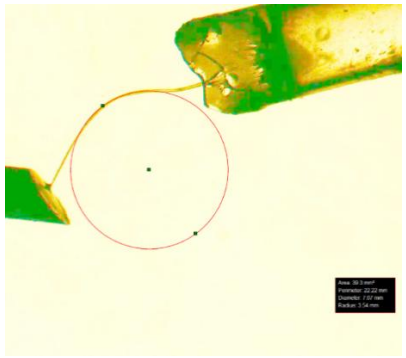

***ε* = 0.074/ 7.07 = 1.05 %**

Stage-2

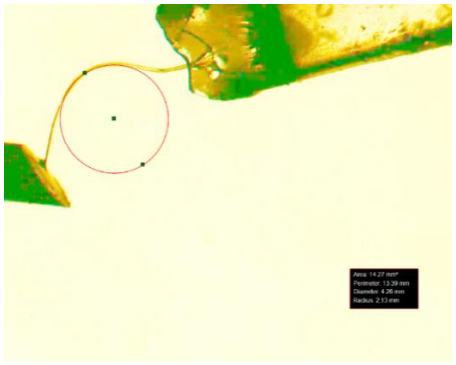

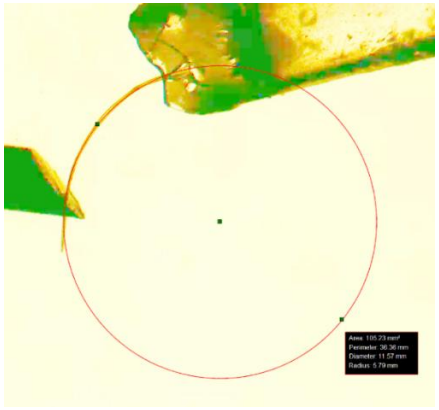

Elastic recovery = ~ 1.1%

Stage-3

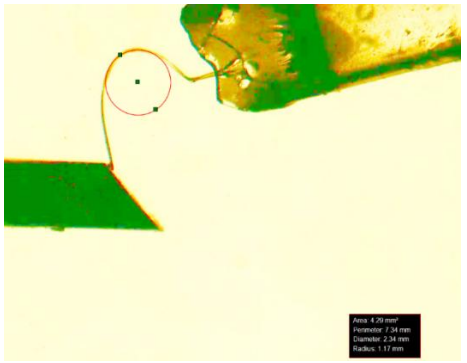

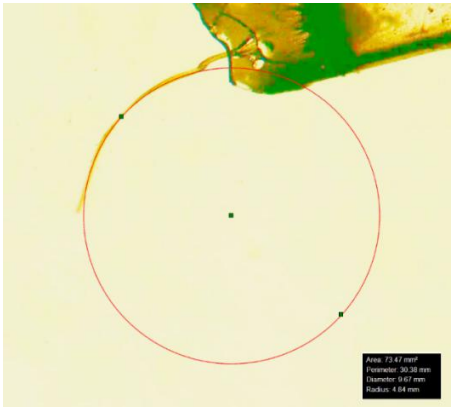

Elastic recovery = ~ 2.39%

Fig. S10 Calculation of elastic strain, percentage of elastic recovery after plastic deformation at the different stagesof the mechanical bending of OXC.

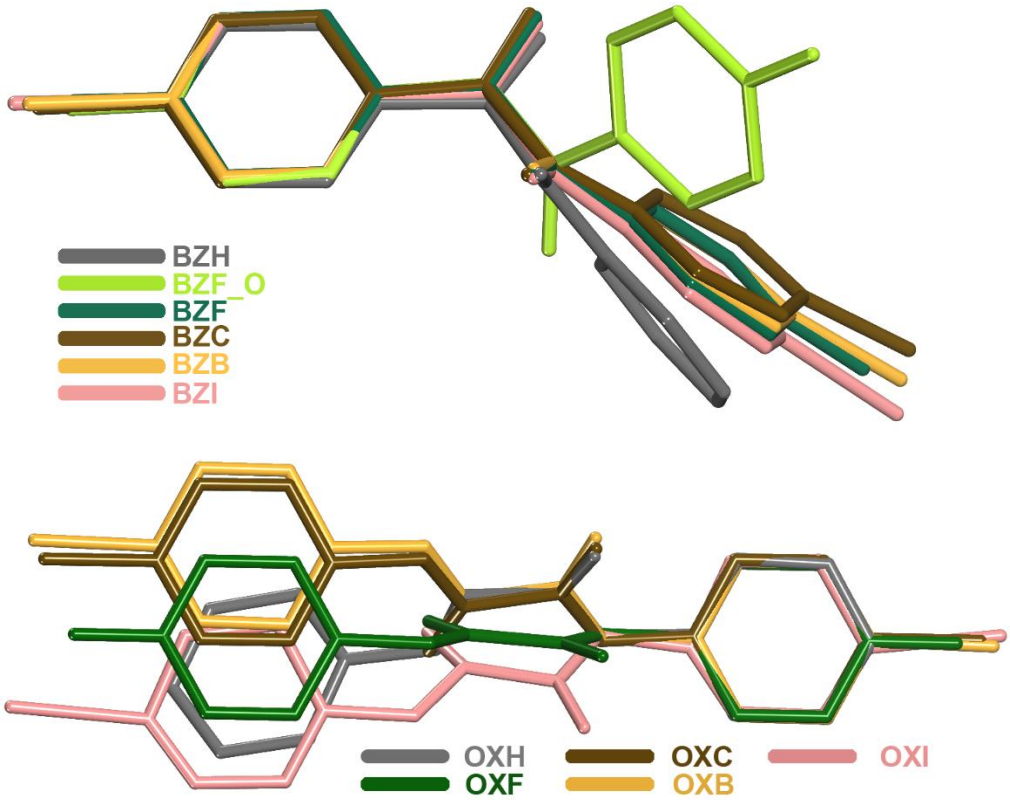

Fig. S11 Overlap images to compare the conformational preferences adopted by (a) benzils and (b) oxalates

Table S5 The torsional twist adopted by the phenyl rings in the compounds

Compound		Phenyl twist angle (°)
OXH		22.56
OXF		0
OXC		0
OXB		0
OXI	Type 1	2.69
	Type 2	1.36
BZH		76.77
BZF_O		64.74
BZF		57.65
BZC		53.72
BZB		57.28
BZI		60.97

BZH

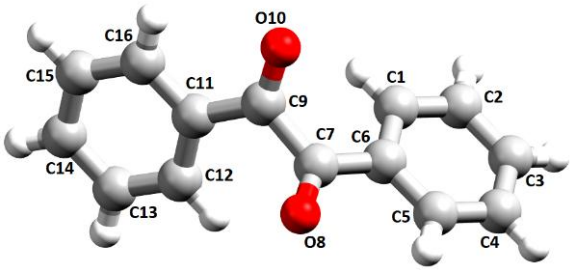

BZF

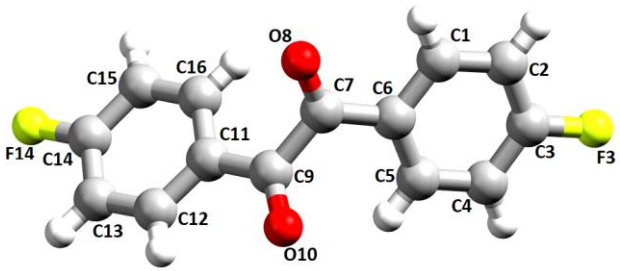

BZC

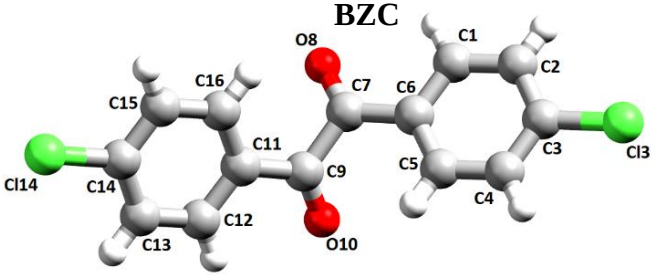

BZB

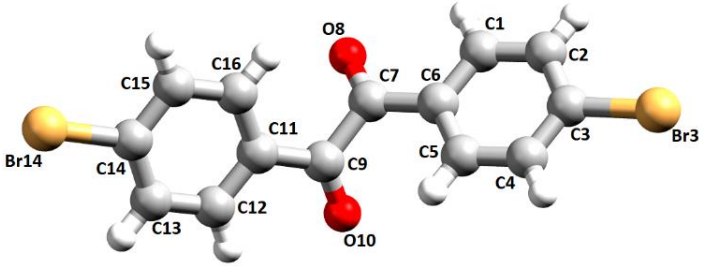

BZI

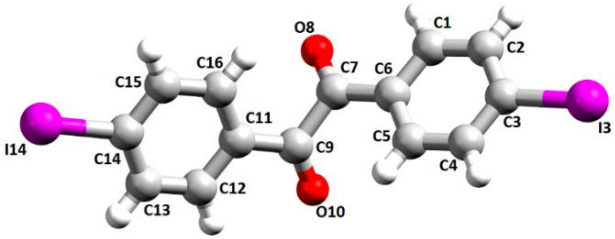

OXH

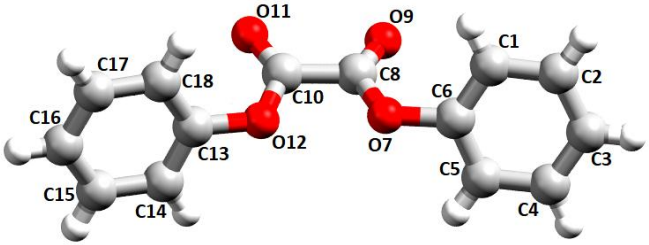

OXF

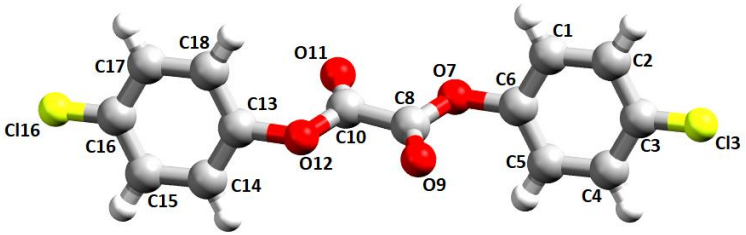

OXC

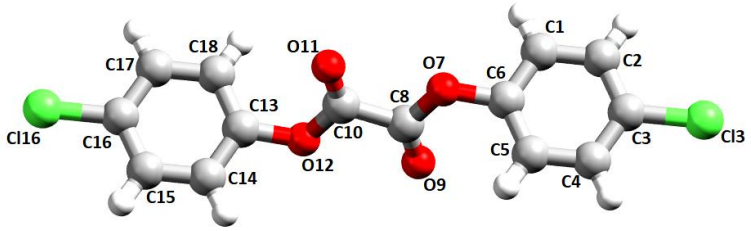

OXB

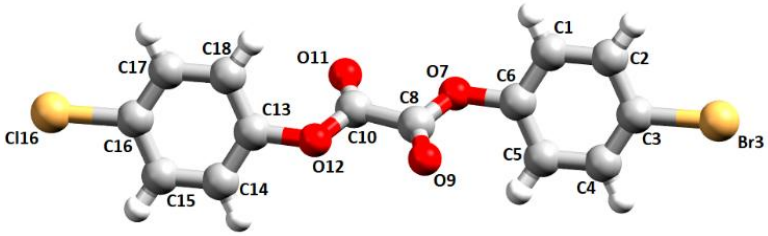

OXI

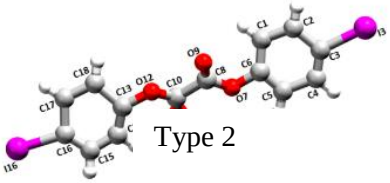

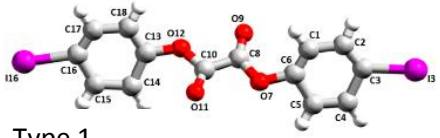

Table S6 Torsion angles adopted by the benzil and oxalate compounds

Torsion angles adopted by the benzil compounds

Torsion angle	Compound					
	BZH	**BZF_O**	**BZF**	**BZC**	**BZB**	**BZI**
O = C-C = O	107.4(2)	-110.6(1)	117.0(2)	118.5(1)	116.1(3)	114.6(4)
C(6)-C(7)-C (9)-C(11)	115.3(1)	-119.6(1)	127.2(2)	131.6(1)	127.8(3)	125.4(4)
C(5)-C(6)-C (7)-C(9)	172.2(1)	11.0(2)	-5.3(3)	-6.5(2)	-6.0(4)	-7.8(5)
C(5)-C(6)-C (7)-O(8)	-3.5(2)	-174.3(1)	-179.8(2)	-179.5(1)	-179.8(2)	178.0(4)
C(1)-C(6)-C (7)-O(8)	174.8(1)	5.7(2)	-0.1(3)	-0.2(2)	-1.1(4)	-1.2(6)
C(6)-C(7)-C (9)-O(10)	-68.7(2)	64.4(1)	-57.9(3)	-55.0(2)	-58.1(3)	-60.0(5)

Torsion angles adopted by the oxalate compounds

Torsion angle	Compound					
	OXH	**OXF**	**OXC**	**OXB**	**OXI**	
					Type 1	Type 2
O_C-C-C-O_C	-8.8(3)	180	180	180	172.0(2)	175.0(2)
O = C-C = O	-8.5(4)	180	180	180	168.0(3)	168.0(2)
O_C (7) = C(8)-C(10)-O(11)	172.0(3)	-0.4(3)	-1.0(3)	-0.28 /0(1)	-3.0(4)	-4(3)
O_C (12) = C(10)-C(8)-O(9)	170.7(3)	0.4(3)	1.0(3)	0.28	7.0(4)	-13.0(3)
C(6)-O(7)-C (8)-O(9)	3.4(4)	-2.0(3)	-2.2(3)	-3.0(1)	1.0(4)	14.0(4)
C(13)-O(12)-C (10)-O(11)	0.5(4)	2.0(3)	2.2(3)	3.0(1)	-20.0(3)	-6.0(3)
C(8)-O(7)-C (6)-C(5)	-118.0(3)	70.3(3)	60.5(3)	57.8(9)	-138.0(2)	-135.0(2)
C(10)-O(12)-C (13)-C(14)	112.2(3)	-112.6(2)	-124.2(2)	126.1(7)	-32.0(3)	-45.0(3)

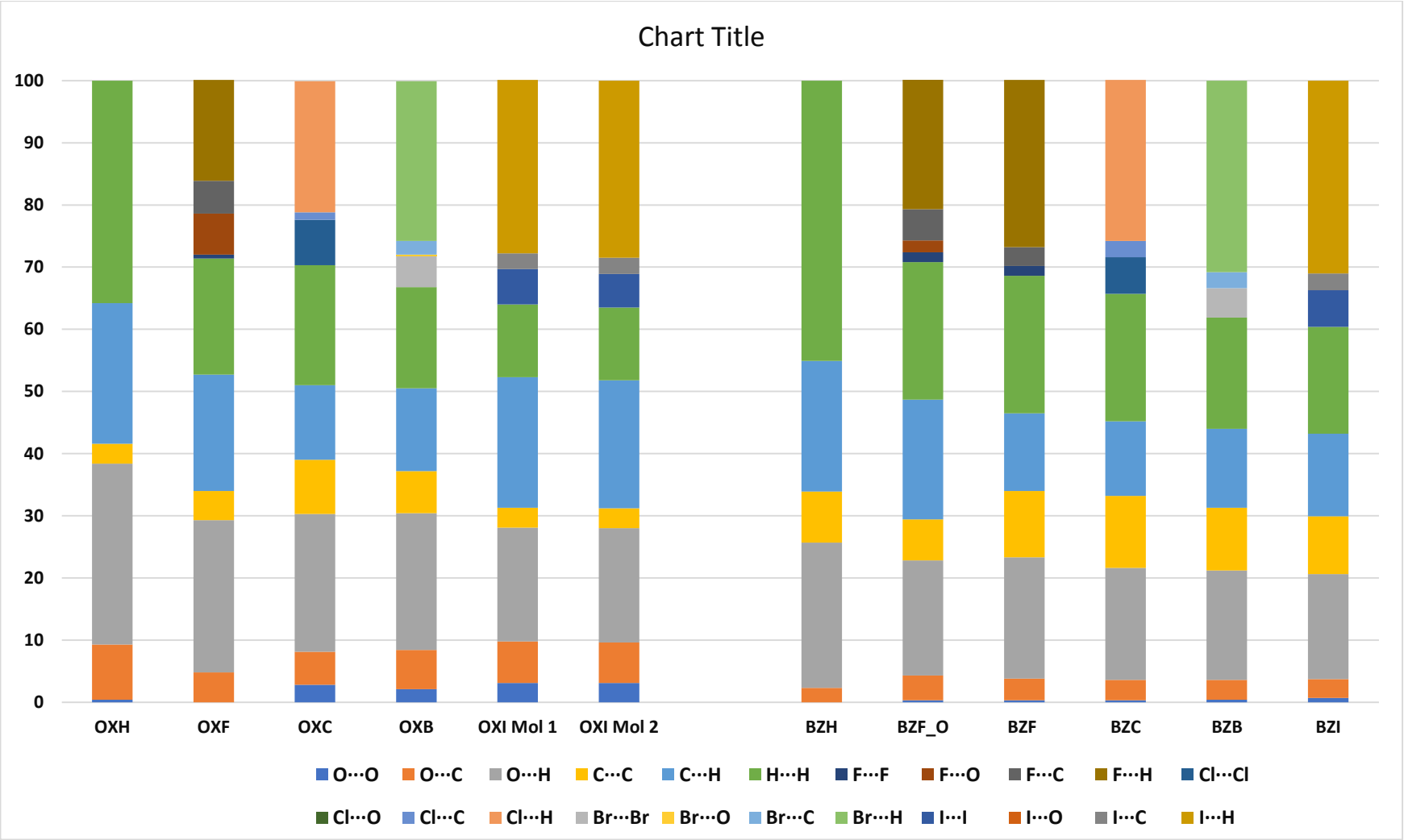

Fig. 12 The relative contribution of interactions, as derived from the Hirschfeld analysis.

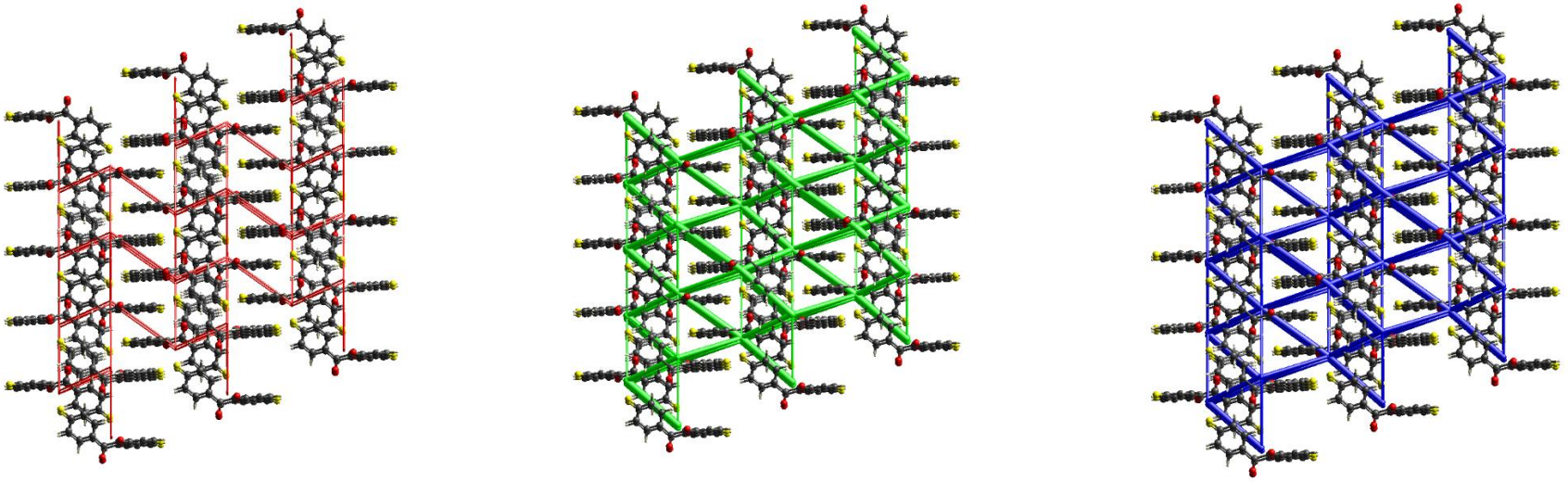

Fig. S13 The energy frameworks of BZF_O. The electrostatic, dispersive, and total energy are represented in red, green, and blue tubes. The size of the tubes is related to the strength of the interactions.

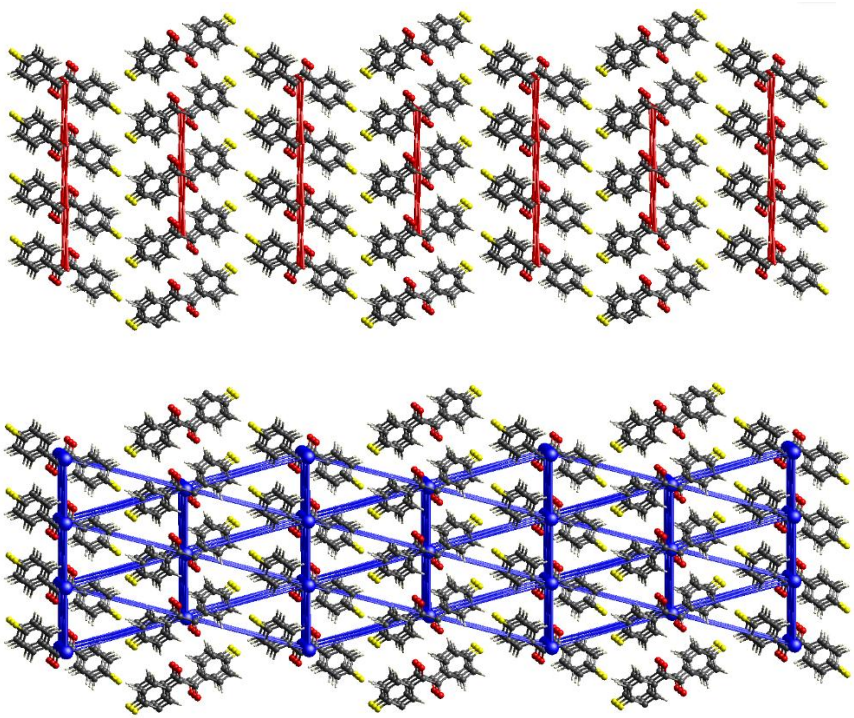

Fig. S14 The energy frameworks of BZF. The electrostatic, dispersive, and total energy are represented in red, green, and blue tubes. The size of the tubes is related to the strength of the interactions.

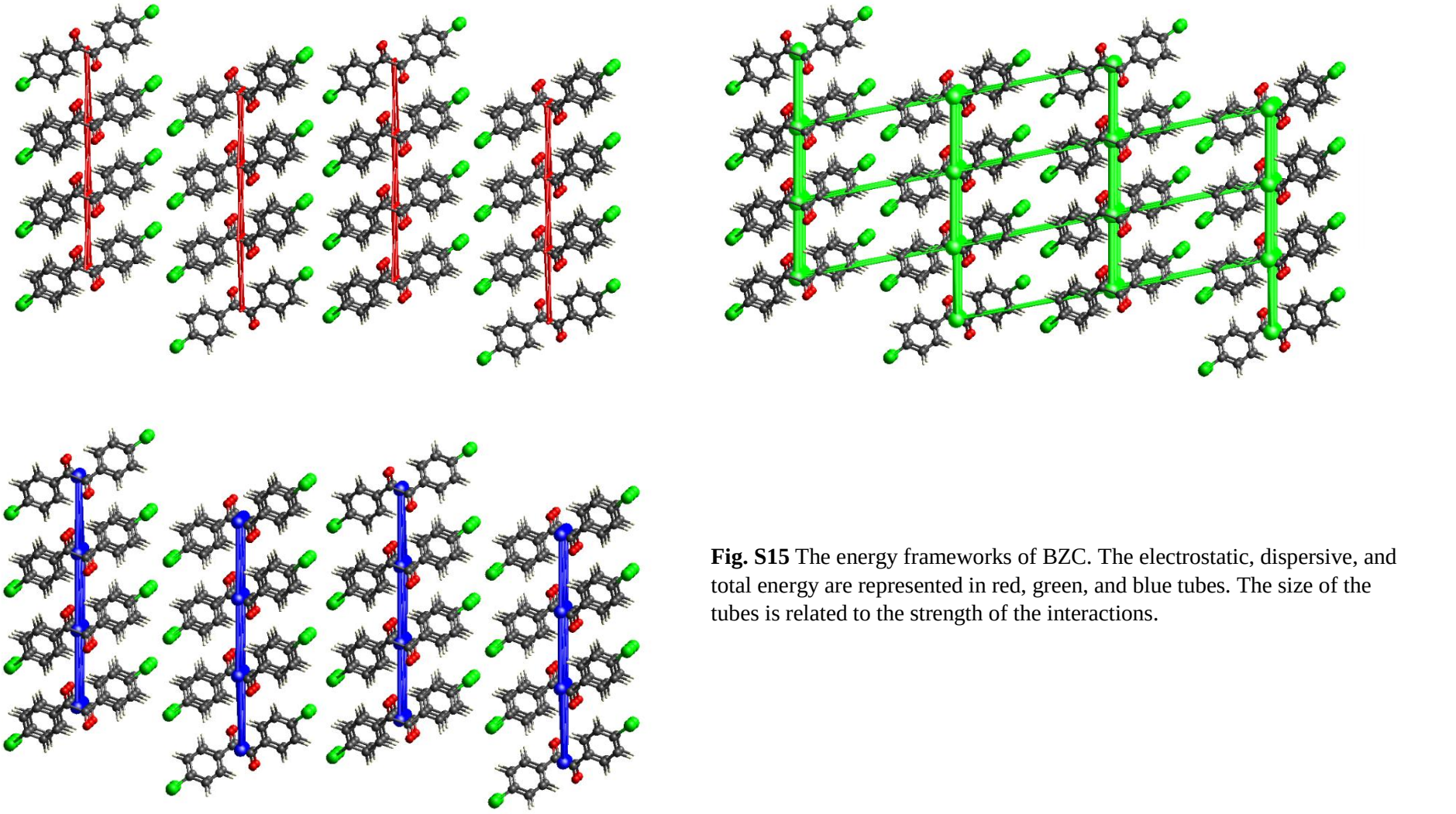

Fig. S15 The energy frameworks of BZC. The electrostatic, dispersive, and total energy are represented in red, green, and blue tubes. The size of the tubes is related to the strength of the interactions.

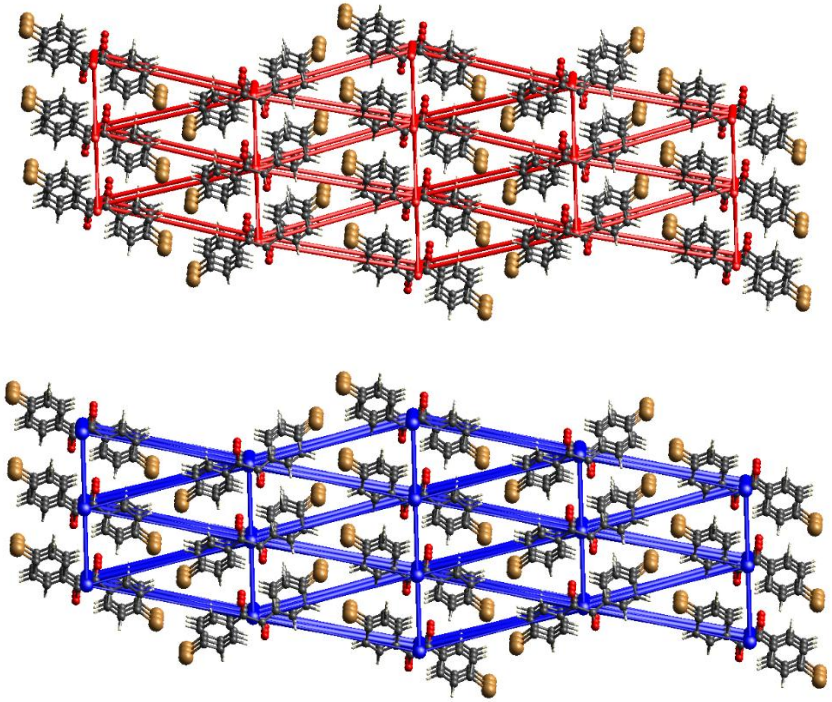

Fig. S16 The energy frameworks of BZB. The electrostatic, dispersive, and total energy are represented in red, green, and blue tubes. The size of the tubes is related to the strength of the interactions.

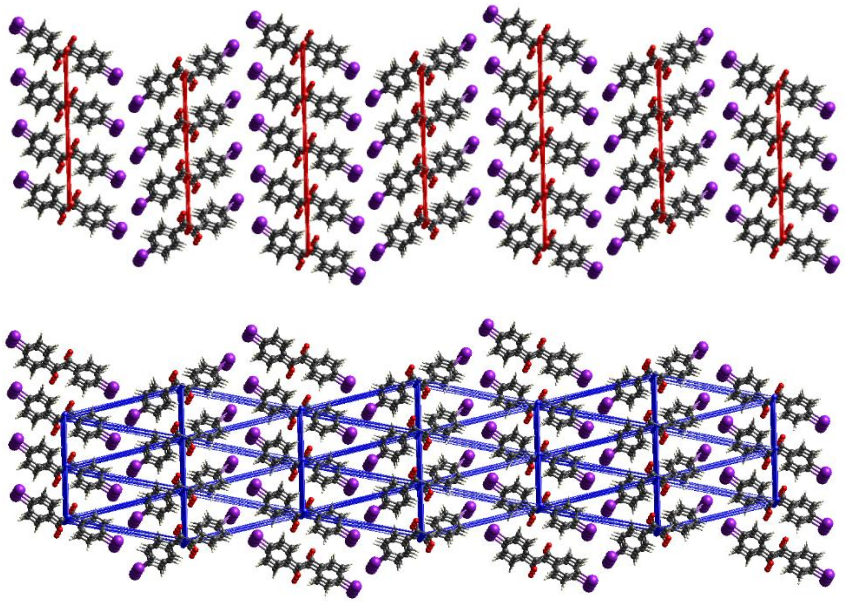

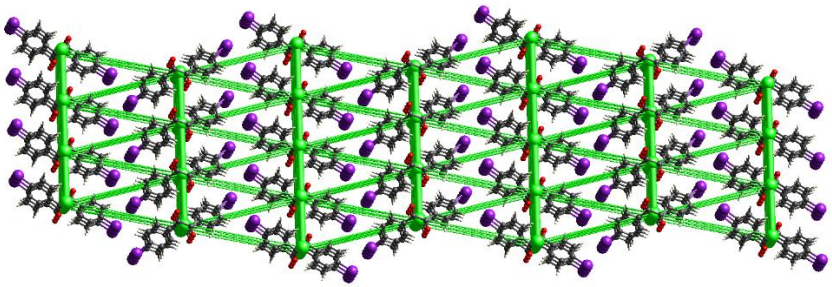

Fig. S17 The energy frameworks of BZI. The electrostatic, dispersive, and total energy are represented in red, green, and blue tubes. The size of the tubes is related to the strength of the interactions.

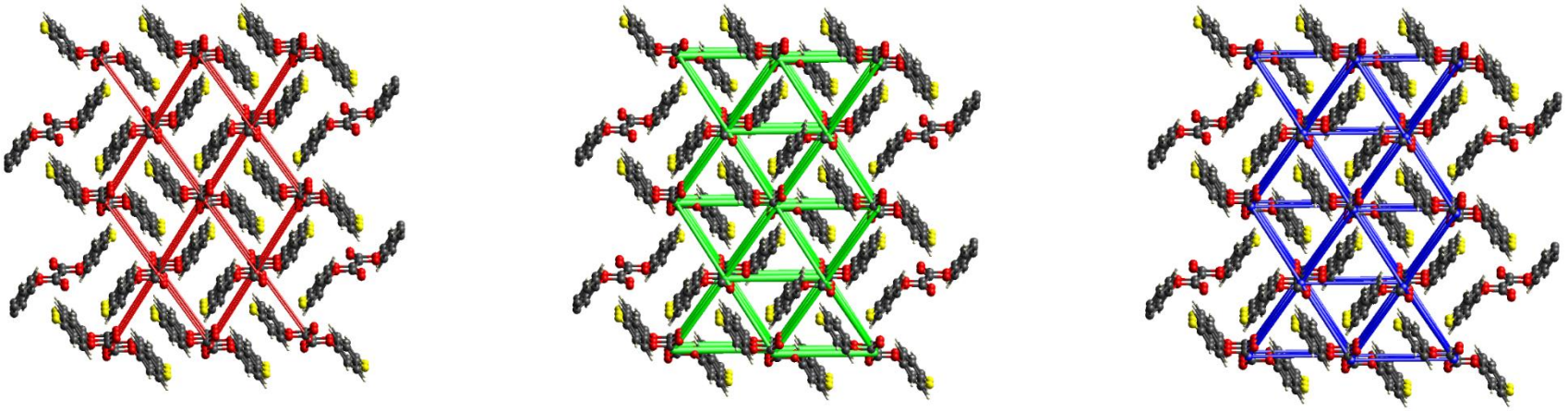

Fig. S18 The energy frameworks of OXF. The electrostatic, dispersive, and total energy are represented in red, green, and blue tubes. The size of the tubes is related to the strength of the interactions.

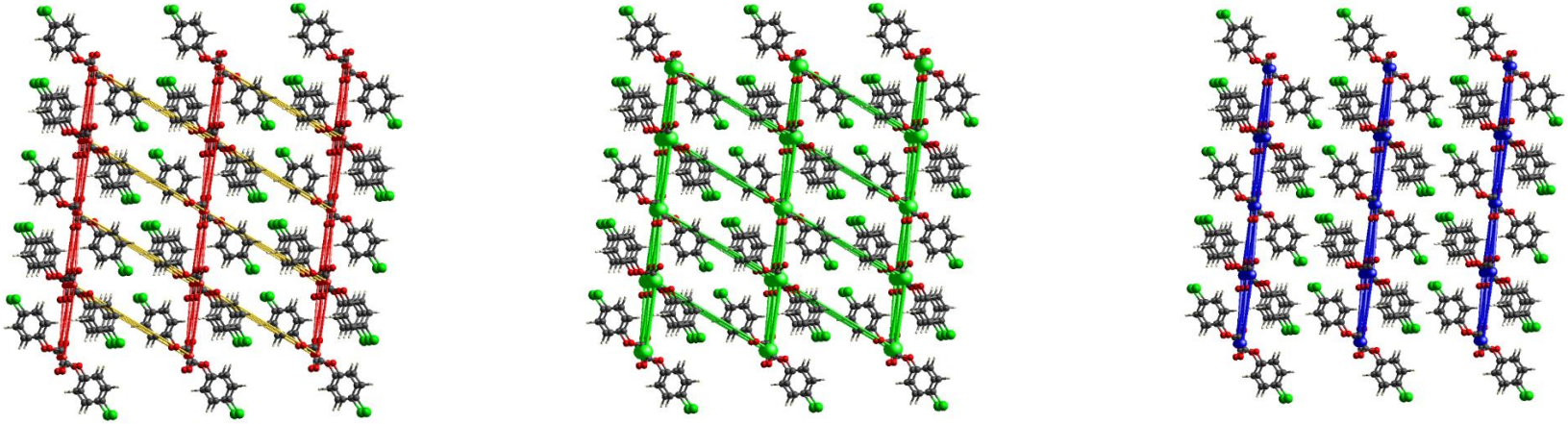

Fig. S19 The energy frameworks of OXC.

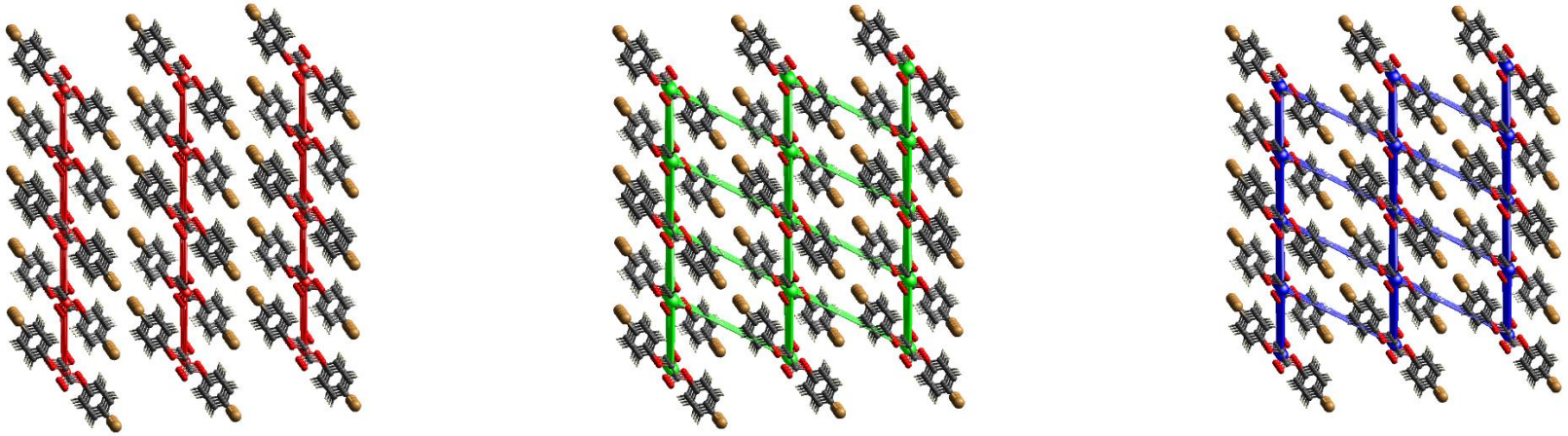

Fig. S20 The energy frameworks of OXB.

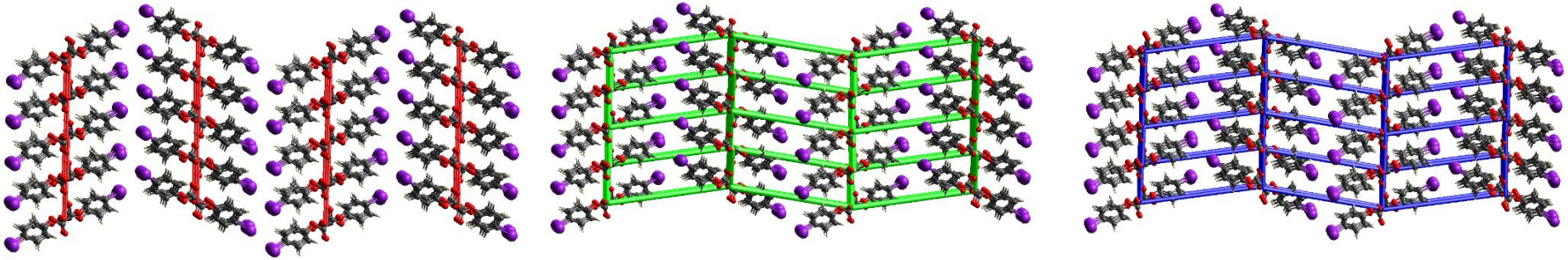

Fig. S21 The energy frameworks of OXI.

Table S7. Calculated normalized contacts (*Nc*) values of the halogen interactions in the interlayer region

Compound	*d*	*Vr*	*Nc*
BZF		2.94	
BZC	3.366	3.5	0.961714
BZB	3.845	3.7	1.039189
BZI	3.96	3.96	1
OXC	3.587	3.5	1.024857
OXB	3.51	3.7	0.948649
OXI	4.037	3.96	1.019444

d = bond distance; *V*r = sum of van der Waals radii; *Nc* = normalized contacts

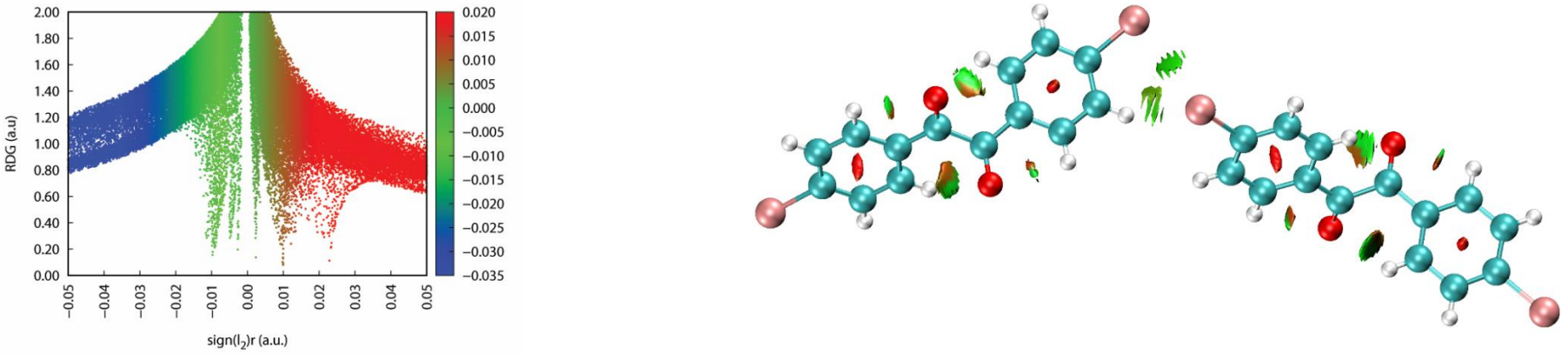

Fig. S22 The RDG plot of BZB. The scatter plot of the RDG versus the electron density multiplied by the sign of the second Hessian eigenvalue(λ2) and the RDG isosurface of the nearest interacting molecules in the interlayer region with the differences in the interactions that resembles in the scatter plot.

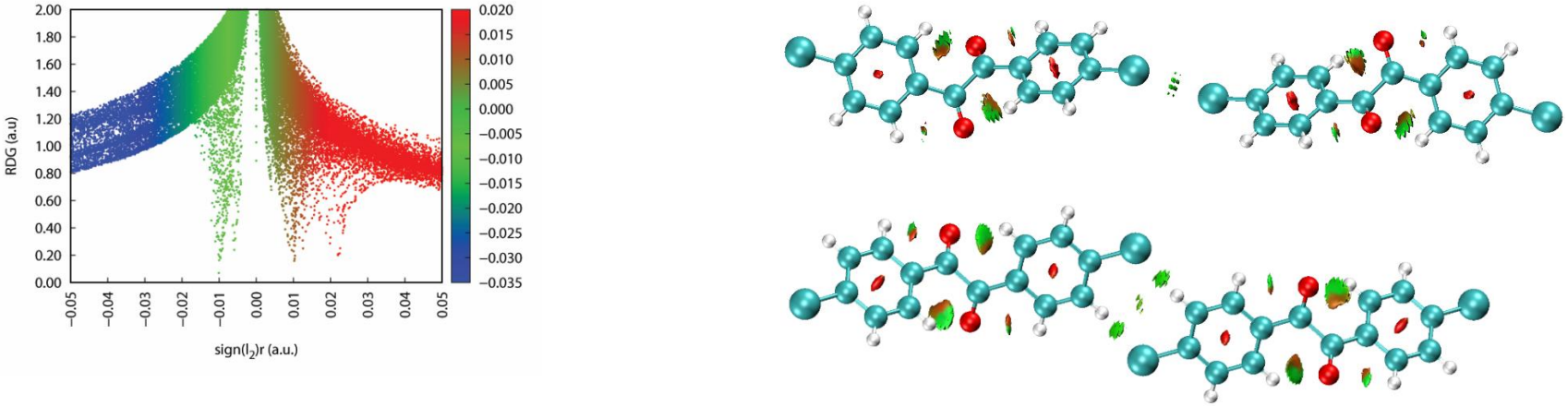

Fig. S23 The RDG plot of BZC.

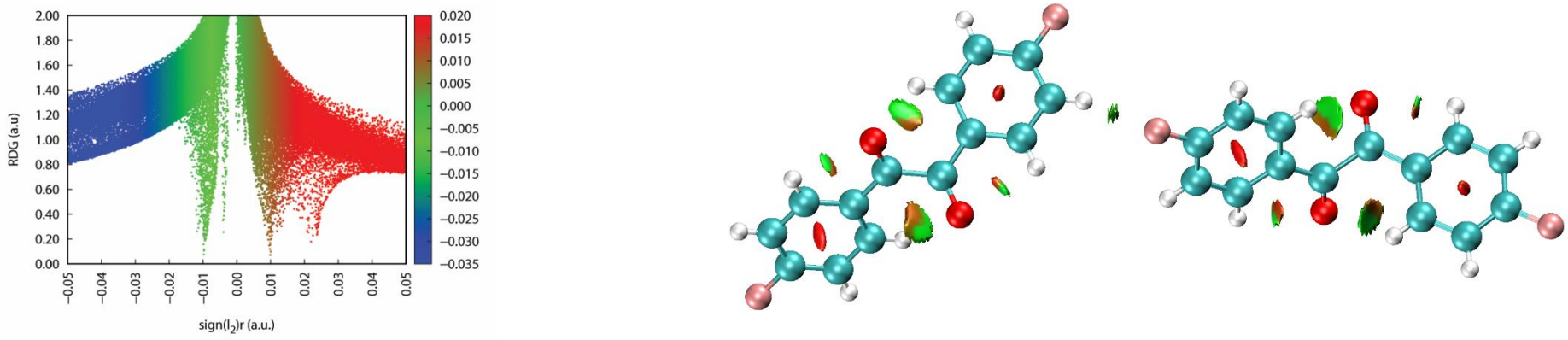

Fig. S24 The RDG plot of BZF.

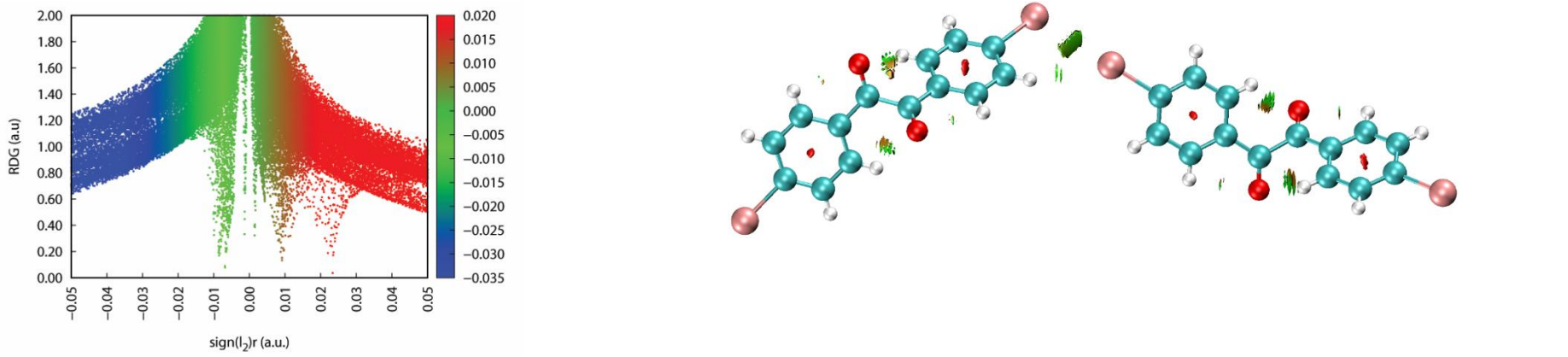

Fig. S25 The RDG plot of BZI.

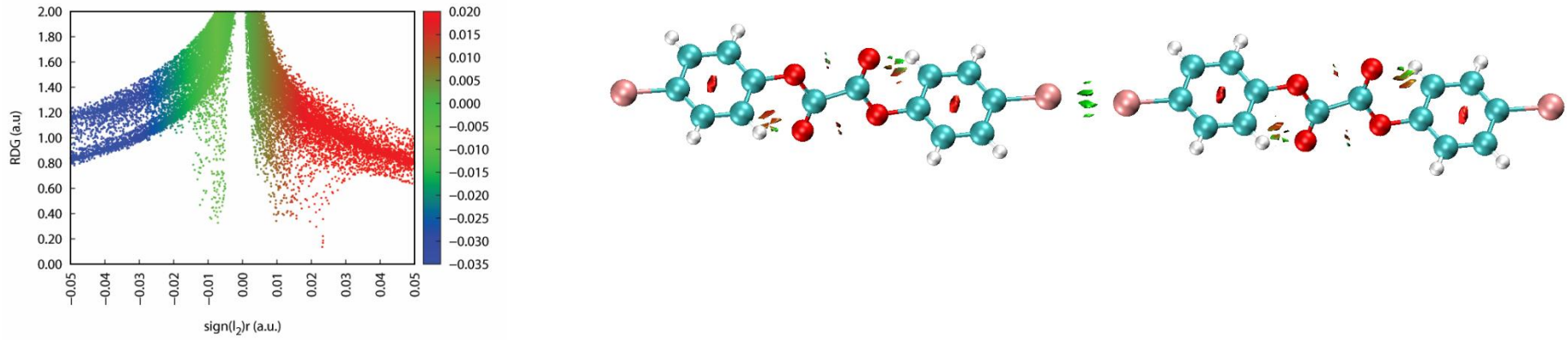

Fig. S26 The RDG plot of OXB.

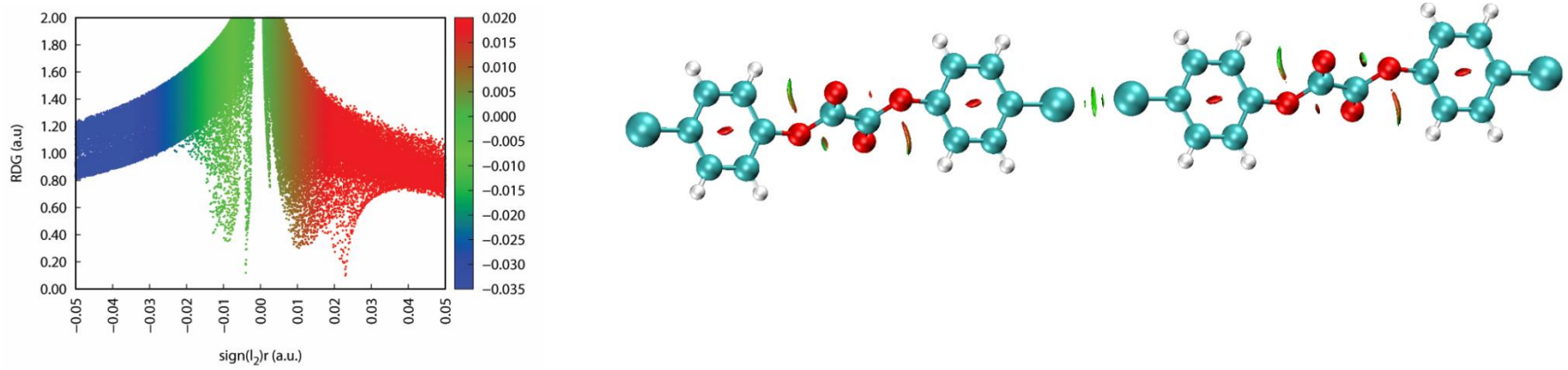

Fig. S27 The RDG plot of OXC.

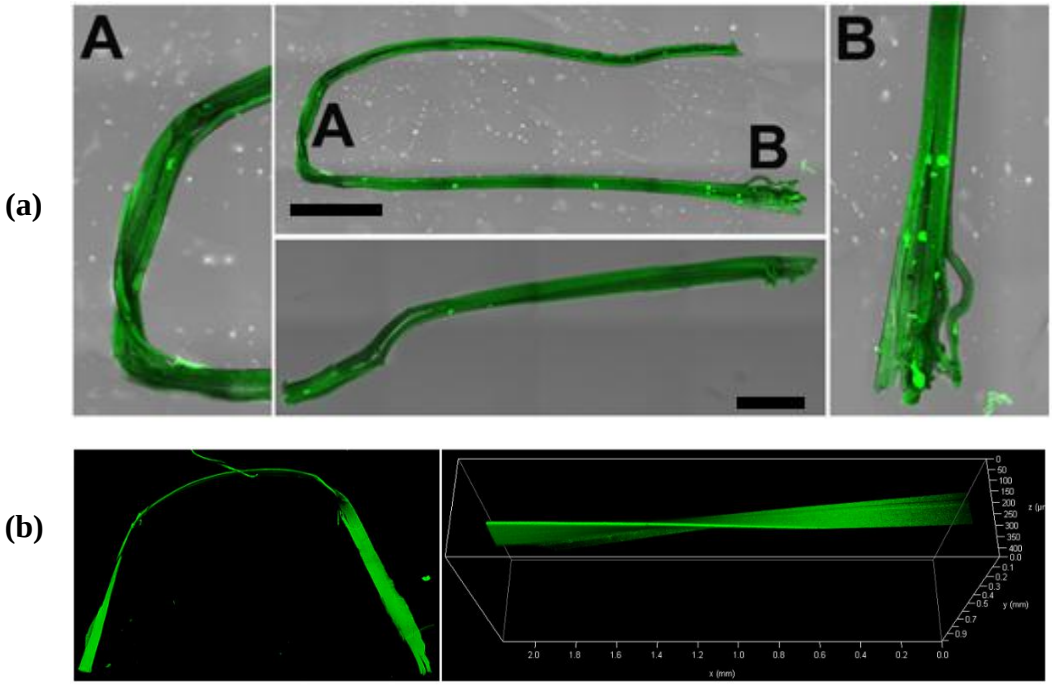

Fig. S28 The confocal microscopy images. (a) the bent crystal of BZC. Note the delamination observed in the area corresponding to the ends and the bent region (the scale corresponds to 1 mm). (b) The bending and twisting are observed in BZF.

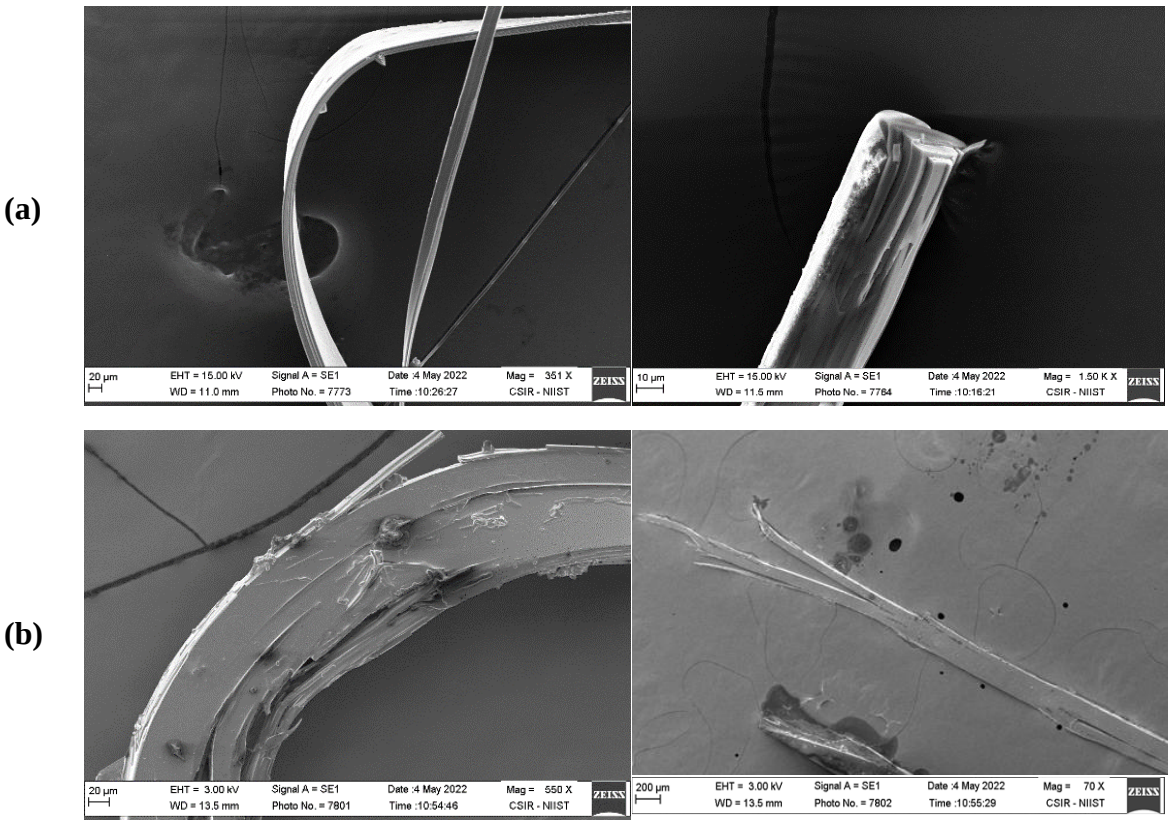

Fig. S29 Scanning Electron Microscopy images. (a)The bent portion and the tip of BZC crystal. (b) The bent portion and tip of OXC crystal.

Diffraction experiments on the bent crystals

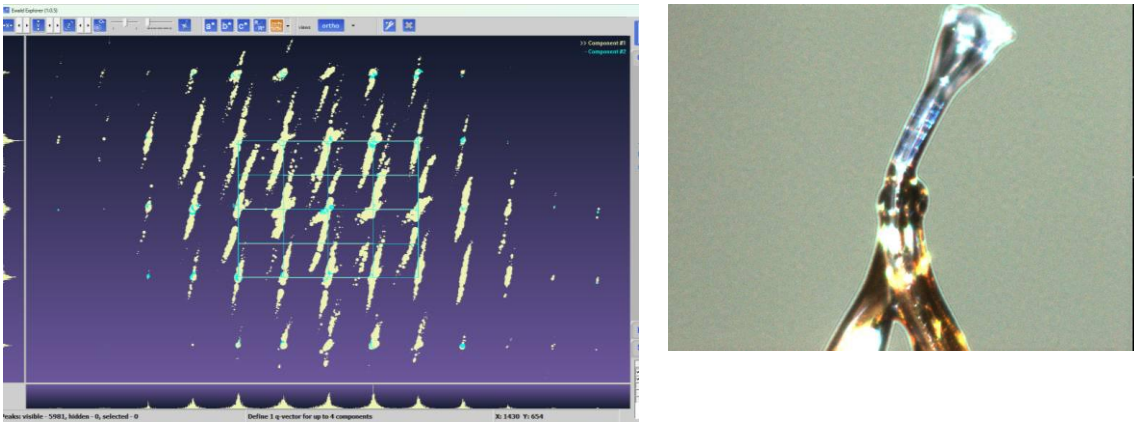

Fig. S30 The diffraction patterns obtained form BZB.

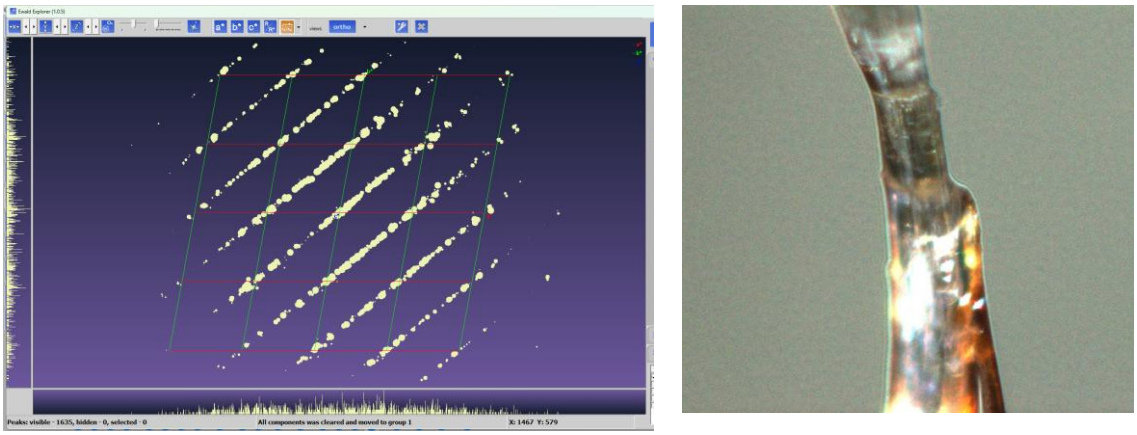

Fig. S31 The diffraction patterns obtained form BZC.

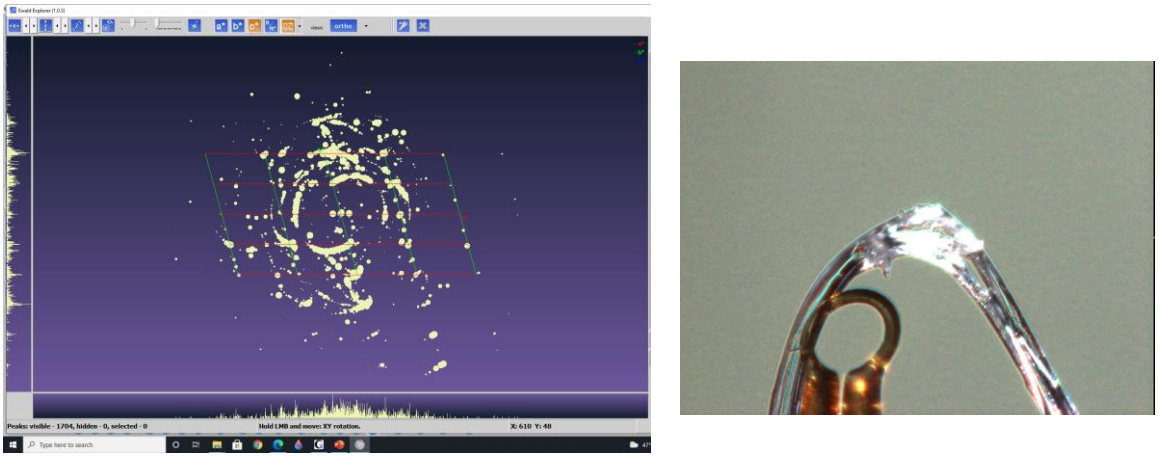

Fig. S32 The diffraction patterns obtained form OXC.

Absorption and Emission spectra of crystals

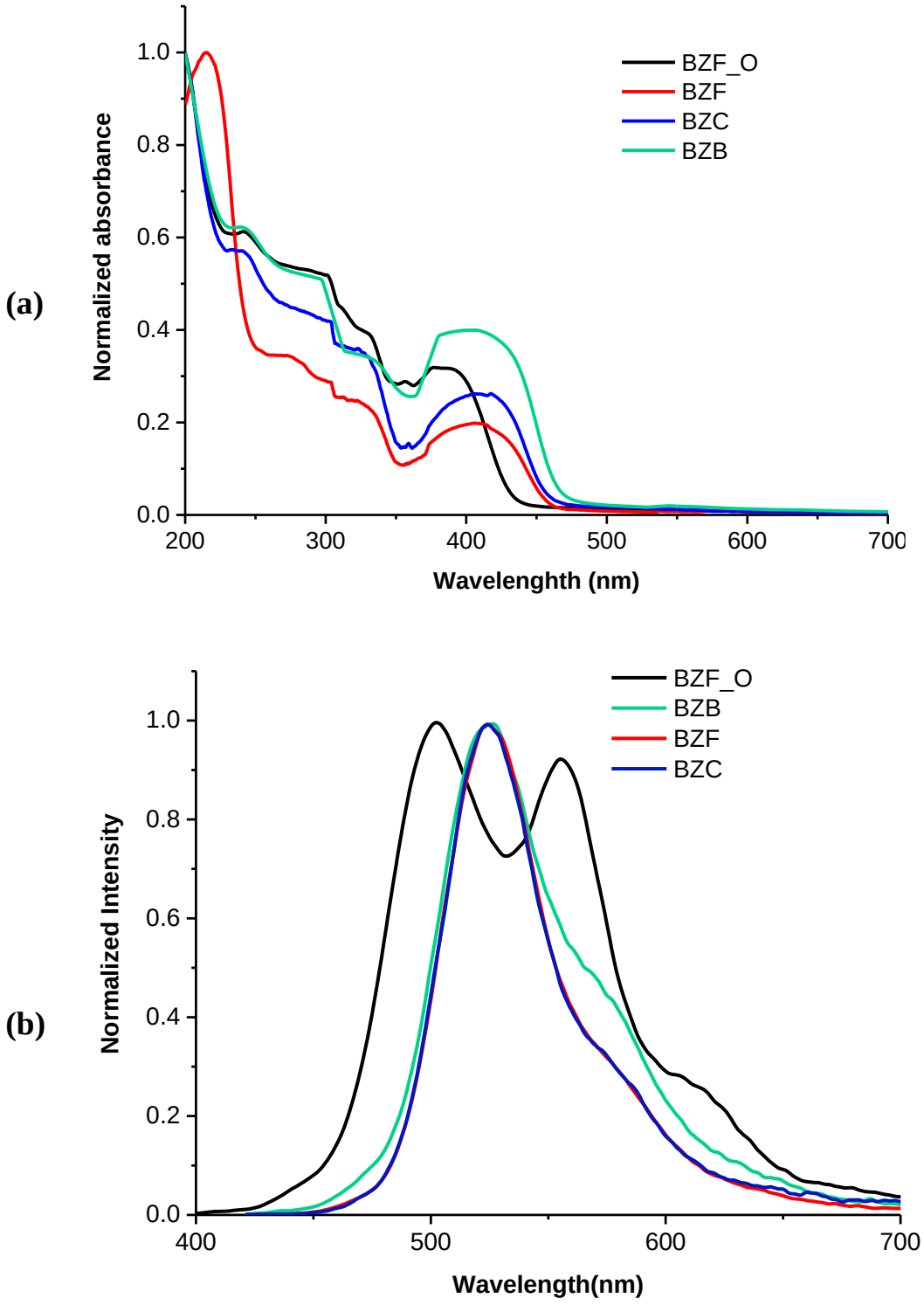

Fig. S33 Absorption and emission spectra of solid crystalline samples of benzil compounds.